2021 43rd Annual International Conference of the
IEEE Engineering in Medicine & Biology Society (EMBC)
Oct 31 - Nov 4, 2021. Virtual Conference

A Semi-Automated System for Wafer-Scale Optical Waveguide Characterization*

Ramgopal Venkateswaran, Jay W. Reddy, and Maysamreza Chamanzar, *Member, IEEE*

***Abstract*— Integrated photonic waveguide systems are used in biomedical sensing and require robust, high-throughput methods of characterization. Here, we demonstrate a semi-automated robotic system to characterize waveguides at the wafer-scale with minimal human intervention based on imaging the outscattered light to measure the propagation loss. We demonstrate automated input coupling efficiency optimization using closed-loop control of the input fiber position. The automated characterization system collects and combines multiple images of the waveguide to measure the propagation loss. This system allows high-throughput characterization of integrated photonic waveguides and lays the foundation for a fully automated and high throughput system to characterize photonic waveguides at the wafer scale.**

***Clinical Relevance*— This method enables high precision, high throughput characterization of optoelectrical neural probes to maximize the yield of surgical implantation and electrophysiology recording.**

I. Introduction

Integrated photonic waveguides are utilized in a variety of implantable devices for biomedical sensing and stimulation [1]. In neuroscience, neural probes are required for light delivery deep into brain tissue for techniques such as functional fluorescence imaging and optogenetics [2]–[4]. In addition to traditional materials for realizing integrated photonic waveguides, flexible, biocompatible material platforms such as Parylene photonics have been developed to address the unique needs of neural interfaces [5], [6].

Multiple methods have been developed to characterize the propagation loss in photonic waveguides, including the cutback method [7] and the resonator Q fitting method [8]. While these methods have been applied successfully in the past, the cutback method is destructive and the resonator method requires the design and integration of microresonators to measure loss. In many photonic applications, it is necessary to individually test and validate each optical channel. Therefore, a nondestructive, in-situ characterization scheme is desired. The difficulty of characterization is exacerbated by the necessities of implantable biophotonic designs, which require sparsely and irregularly arranged output ports in different configurations to match anatomical structures for a particular experiment. Therefore, standardized test fixtures are difficult to design, and a versatile, high-degree-of-freedom system is required. Lastly, for mass production of such devices, wafer-scale characterization capabilities are desired.

For these reasons, we prefer the outscattered light method, which computes the propagation loss in the waveguide based on measurements of outscattered light intensity along the length of the waveguide. For light confined and propagating in a waveguide structure, optical power decays due to either material absorption or scattering losses due to internal defects or sidewall roughness. Outscattered light contributes to waveguide loss but may also be imaged via external optics to analyze a waveguide structure. The intensity of light scattered out of the waveguide is proportional to the propagating optical power and the local defect density or sidewall roughness. Assuming uniformity of defects and sidewall roughness throughout the waveguide and a steady-state mode power distribution, the intensity of outscattered light will decay with the same exponential loss coefficient as the confined light. In this way, we can analyze the losses in a waveguide via imaging with a charge-coupled-device (CCD) camera.

However, manual alignment of the light source to the waveguide input facet and subsequent image capture are still tedious and low-throughput, and hence, not suitable for high-throughput wafer-scale analysis. In this paper, we demonstrate a system capable of semi-automated alignment and measurement of loss from a waveguide for wafer-scale characterization (Fig. 1).

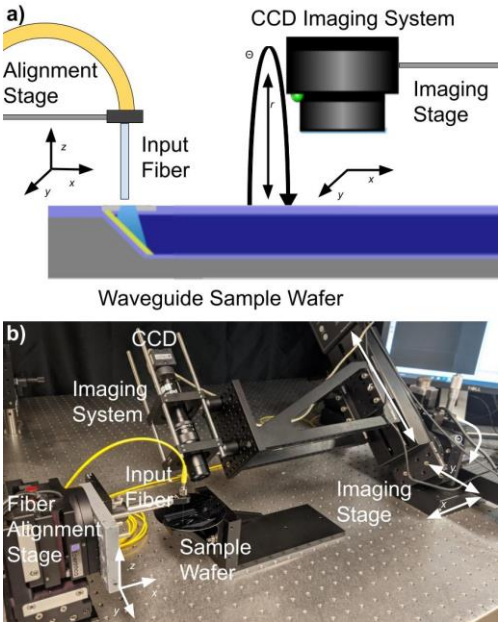

Figure 1: a) Schematic diagram consisting of an input fiber with 3-

*Research supported by the National Science Foundation under Grant No. 1926804 and National Institutes of Health under award No. 1RF1NS113303.

R. Venkateswaran is with the Department of Electrical and Computer Engineering, Carnegie Mellon University, USA (e-mail: ramgopav@andrew.cmu.edu)

J. Reddy is with the Department of Electrical and Computer Engineering, Carnegie Mellon University, USA (e-mail: jreddy1@andrew.cmu.edu)

M. Chamanzar is with the Department of Electrical and Computer Engineering, Carnegie Mellon University, USA (phone: 412-268-3390, email: mchamanz@andrew.cmu.edu)

dimensional (x,y,z) motorized alignment capabilities, the waveguide sample wafer, and an output imaging system with 4-dimensional (x,y,r,θ) motorized alignment capabilities. b) Annotated photograph of the characterization system schematically illustrated in (a).

II. Methods

A. Waveguide Preparation and System Construction

Parylene photonic waveguides with embedded micromirrors for vertical input/output coupling were fabricated at the wafer scale as described in [6]. Waveguides were arranged in arrays of up to 15 waveguides of various widths (5, 10, 15, 30 μm) and lengths (from 5 mm to 5 cm) on a single wafer.

The characterization system comprises four separate modules combined sequentially to form a high-throughput pipeline. First, a micromanipulator (PatchStar, Scientifica) is used to align a single mode fiber (λ = 633 nm) to the input port of a waveguide. The fiber input-coupling stage is a high-precision (20 nm x,y,z step size) and high-stability (< 1 μm drift over 2 hours) micromanipulator. Closed-loop input coupling optimization is carried out by monitoring the outscattered light intensity on a CCD camera (EO-5012M, Edmund Optics). At optimal coupling, the camera is scanned by using a linear stage (NRT150, Thorlabs) along the waveguide length to capture images of the outscattered light. The NRT150 stage has a rated absolute on-axis accuracy of 19.29 μm. Therefore, the imaging stage position alone is not sufficient for pixel-perfect accuracy. To correct for any positioning error in the imaging stage, multiple captured images are stitched together based on their overlapping regions to form a single high-resolution image along the entire waveguide length. The propagation loss for the waveguide is extracted from this image by measuring the overall intensity decay of outscattered light.

The following subsections will discuss the propagation loss measurement and the automated input fiber alignment.

B. Propagation Loss from a High-Resolution Image

The pixel intensity values from a CCD camera image corresponding to outscattered light are extracted along the waveguide axis. Then, the data is fit to a decaying exponential using the method of least squares. The attenuation coefficient is used to characterize the propagation loss in the waveguide.

The waveguide trajectory is identified from the image by de-noising the image with a median filter, finding the row corresponding to the brightest pixel in each column of the image, and fitting a line to these datapoints (Fig. 2a). The Random Sample Consensus (RANSAC) algorithm is used to fit the line. It uses iterated random sampling of the data-points to identify outliers and leaves them out for estimating the line parameters [9]. This makes it particularly well-suited for this data, which includes images containing reflections and noise that are unrelated to the waveguide, as well as images where the waveguide trajectory does not span all columns of the image. After the initial fit obtained by running the RANSAC algorithm, the image is cropped to only the columns spanned by the waveguide (as indicated by the fit), and the RANSAC algorithm is run again on the cropped image with a lower fitting threshold. This further increases the accuracy and prevents spurious fits by discarding the influence of irrelevant columns on the overall fit, with minimal increase in computational time.

The image is then rotated such that the identified waveguide trajectory is horizontal, and cropped to have a 500 px height, with 250 px on either side of the trajectory line (Fig. 2b). The pixel values in the image are summed column-wise. The pixel distance values are converted to physical distance values using the known scaling of the imaging system. This dataset gives an estimate of the outscattered light intensity (proportional to the summed pixel values) along the length of waveguide, which is fitted to a decaying exponential to obtain the attenuation coefficient (Fig. 2c).

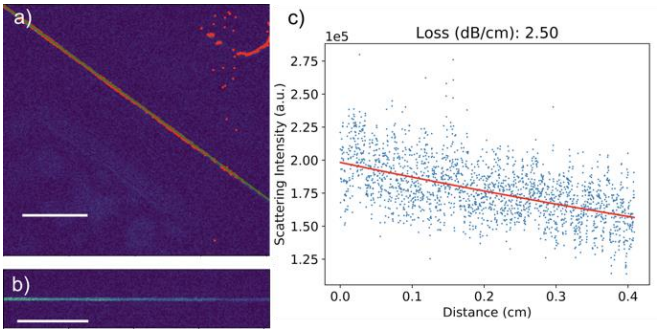

Figure 2: Scattering Loss Extracted from a Single Image; a) identified path of waveguide (in green), superimposed on highest intensity rows for each column (in red) – both axes are in pixels; b) rotated and cropped image centered on waveguide path – axis also in pixels; c) plot of scattering intensity vs distance. Scale bars indicate 1 mm.

The intensity decay can be modeled as $I = I_0 e^{-\alpha x}$, where I is the light intensity at distance x from the input facet of the waveguide, I_0 is the initial light intensity, and α is the attenuation coefficient.

It should be noted that in large multimode waveguides, such as those measured here, light can propagate in multiple modes of the waveguide, which will experience different propagation losses. In general, lower-order modes are highly confined and experience less loss due to surface scattering compared to higher-order modes, which tend to experience higher propagation loss and are quickly attenuated. Power coupling between modes occurs due to perturbations in the waveguide such as imperfections due to surface roughness. Over a long propagation length, the modal power distribution will converge to a steady-state, and the overall waveguide loss will be a superposition of the losses of individual modes [10]. All measurements for waveguide loss and alignment are performed at least 1 cm from the input facet to allow the power distribution in the waveguide to reach steady-state.

C. Stitching Multiple Images Together

To obtain a high-resolution image of the whole waveguide, multiple overlapping images along different segments of the waveguide are composed into a single image. The algorithm first takes each pair of adjacent images and computes the appropriate overlap along both axes of the image, after which it stitches all the images in order based on the computed overlaps.

The camera is moved in 1-mm increments along the axis of the waveguide and individual images are captured at each position. Both the movement and image capture are

automated, and the system is programmed with a fiber-camera offset, to avoid collisions between the input fiber and the imaging system during movement.

Given a pair of adjacent images, the line corresponding to the waveguide trajectory within each image is first identified using the method described above – called as the "line-finding" phase of the algorithm. The image is then preprocessed as follows: for each column of the image between the endpoints of the line, sum an area of 250 pixels above and below the line to get the average brightness for the waveguide at that column. The 250-pixel boundary was empirically chosen to capture the outscattered brightness of the waveguide. Next, for every possible candidate horizontal offset, we compute the mean squared error between the column-wise brightnesses computed for the two images if they were to overlap at that offset. Finally, we select the horizontal offset that minimizes this quantity, and compute corresponding vertical offset from the line corresponding to the waveguide trajectory found during the initial "line-finding" phase of the algorithm and stitch the two images accordingly. This process is done sequentially, adding one image at a time to the existing composite image to produce the final full image.

D. Aligning to a Waveguide

To obtain bright enough images from which we can extract the loss data, the system automatically optimizes the coupling of light from a laser into the waveguide's input facet. The fiber tip is manually positioned just above the wafer surface during sample loading. During the measurement, the fiber position is automatically optimized along a plane parallel to the wafer surface until there is sufficient input coupling to obtain a bright image with maximal outscattered light intensity.

The initial search space used in the experiments is a 20 μm by 20 μm square region. Therefore, initial manual alignment must be accurate to within this search space. In general, the initial search space cannot exceed the waveguide pitch, or the algorithm risks converging to an adjacent waveguide rather than the target waveguide. In this study, the waveguide input ports are spaced 40 μm apart in the array, and the search space is chosen to be smaller than this limit.

The optimization algorithm iteratively narrows down this search space – in each step, the fiber is swept over a grid of points within the search space, and an image is taken at each point. The average brightness of the waveguide in each image is computed by locating the waveguide within the image and taking the average of the column-wise brightnesses (described in the section above). For each point internal to the grid, the average of this quantity over itself and its 8 immediate neighboring points is taken; the point with the maximum such value will be the new center point of the search during the next iteration, which will take place at a higher resolution and a smaller grid size.

Three iterations of this algorithm are performed, each with a 10×10 search grid– in the first one, points in the grid are spaced with an (x, y) resolution of (2 μm, 2 μm). In the second and third rounds, points are spaced (0.4 μm, 0.5 μm) and (0.1 μm, 0.2 μm) apart.

III. Results

A. Stitching Multiple Images Together

The image stitching process maps each point along the waveguide, which may appear in multiple adjacent images, to a single corresponding point in the final image. Fig. 3 illustrates how a section of a stitched image was obtained from three adjacent original images. To measure the propagation loss, a series of 20-30 images are stitched to fit the loss over several cm of outscattered light data.

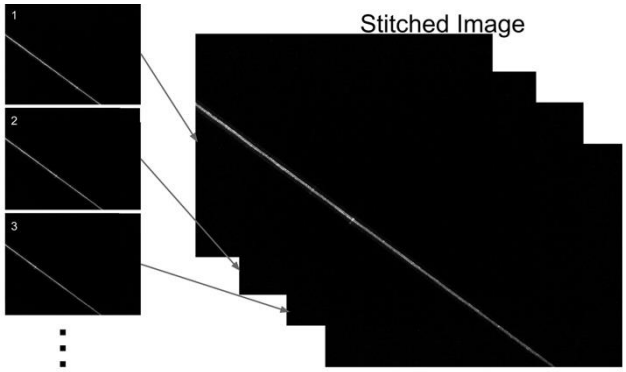

Figure 3: The Effect of Image Stitching; The images on the left are original photos taken by the camera, and the image on the right is the combined image produced by the image stitching algorithm.

B. Aligning to a Waveguide

The algorithm for aligning to a single waveguide is validated by comparing the converged position to a global brightness profile. The brightness profile is generated by raster scanning the fiber position (with respect to the fixed waveguide) and measuring the brightness of the outscattered light from the waveguide corresponding to each fiber position (by imaging a section of it and using the same techniques mentioned previously to determine the brightness of that image).

Fig. 4 shows that if the algorithm is run with a fixed grid resolution of (1 μm, 1 μm), it approaches the position with peak brightness value after a series of iterations. The brightness profile also indicates that achieving a resolution of 1 μm^2 around the peak corresponds to achieving a brightness value that is within 90% of the peak brightness value. This suggests that our algorithm, which attempts an even higher resolution of (0.1 μm, 0.2 μm), is suitable for aligning to within 90% of the peak brightness.

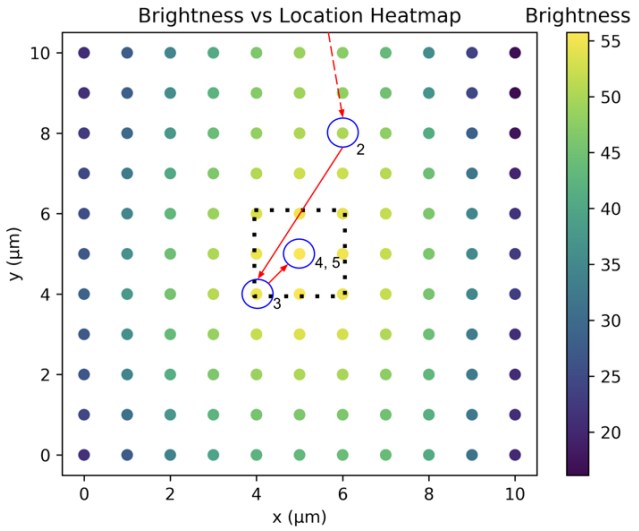

Figure 4: Brightness Profile; 4 iterations of the algorithm, run with a fixed grid resolution of (1 µm, 1 µm). The starting position, at (5, 13), is out of range of the graph; the final positions of each subsequent iteration is labelled with a circle and a number (2 is the position one iteration after the start, 3 is the position 2 iterations after, and so on). The arrows show the transition from iteration to iteration. The dotted box is the target 1 µm^2 region.

IV. Conclusion

The techniques presented in this paper allow for high-throughput characterization of photonic waveguide devices, without the need for additional test structures. This is especially important in implantable biophotonic applications, where device area is highly constrained, geometry is not conducive to a standard testing configuration, and each device must be validated due to the high cost of the device failure and the sensitivity of the experiments, especially the biology experiments involving animal models. Here, we demonstrated a serial alignment and characterization process. Future work could investigate parallelization across the different stages in the process to increase the system throughput. Further development could also extend the waveguide detection and loss fitting methods to account for waveguides which do not follow a straight-line path. Additionally, coarse alignment could be achieved by applying computer vision techniques to detect fiducials on the wafer and perform course alignment.

Such a system can characterize the propagation loss of a single waveguide in fully automated fashion. The fiber may then be repositioned to the input facet of another waveguide, allowing the process to be repeated – this can be done by manual alignment or can itself be automated based on a priori knowledge of the wafer layout. This way, the analysis is scalable to an entire wafer of devices.

Acknowledgment

J.W.R. acknowledges support by the Carnegie Mellon University Ben Cook Presidential Graduate Fellowship, the Carnegie Mellon University Richard King Mellon Foundation Presidential Fellowship in the Life Sciences, the Axel Berny Presidential Graduate Fellowship, and Philip and Marsha Dowd.

References

[1] R. Nazempour, Q. Zhang, R. Fu, and X. Sheng, "Biocompatible and Implantable Optical Fibers and Waveguides for Biomedicine," Materials (Basel)., vol. 11, no. 8, p. 1283, Jul. 2018, doi: 10.3390/ma11081283.

[2] J. W. Reddy, I. Kimukin, Z. Ahmed, E. Towe, and M. Chamanzar, "High density, double-sided, flexible optoelectrical neural probes with embedded micro-LEDs," Front. Neurosci., vol. 13, p. 572, 2019, doi: 10.3389/FNINS.2019.00572.

[3] Y. Son et al., "In vivo optical modulation of neural signals using monolithically integrated two-dimensional neural probe arrays," Sci. Rep., vol. 5, no. 1, p. 15466, Dec. 2015, doi: 10.1038/srep15466.

[4] F. Wu, E. Stark, P.-C. Ku, K. D. Wise, G. Buzsáki, and E. Yoon, "Monolithically Integrated µLEDs on Silicon Neural Probes for High-Resolution Optogenetic Studies in Behaving Animals.," Neuron, vol. 88, no. 6, pp. 1136–1148, Dec. 2015, doi: 10.1016/j.neuron.2015.10.032.

[5] J. W. Reddy and M. Chamanzar, "Low-loss flexible Parylene photonic waveguides for optical implants," Opt. Lett., vol. 43, no. 17, p. 4112, Sep. 2018, doi: 10.1364/OL.43.004112.

[6] J. W. Reddy, M. Lassiter, and M. Chamanzar, "Parylene photonics: a flexible, broadband optical waveguide platform with integrated micromirrors for biointerfaces," Microsystems Nanoeng., vol. 6, no. 1, pp. 1–14, Dec. 2020, doi: 10.1038/s41378-020-00186-2.

[7] I. P. Kaminow and L. W. Stulz, "Loss in cleaved Ti-diffused LiNbO3 waveguides," Appl. Phys. Lett., vol. 33, no. 1, pp. 62–64, Jul. 1978, doi: 10.1063/1.90191.

[8] T. Ito and Y. Kokubun, "Nondestructive measurement of propagation loss and coupling efficiency in microring resonator filters using filter responses," Japanese J. Appl. Physics, Part 1 Regul. Pap. Short Notes Rev. Pap., vol. 43, no. 3, pp. 1002–1005, Mar. 2004, doi: 10.1143/JJAP.43.1002.

[9] M. A. Fischler and R. C. Bolles, "Random sample consensus: a paradigm for model fitting with applications to image analysis and automated cartography," Commun. ACM, vol. 24, no. 6, pp. 381–395, Jun. 1981, doi: 10.1145/358669.358692.

[10] D. Marcuse, "Power Distribution and Radiation Losses in Multimode Dielectric Slab Waveguides," Bell Syst. Tech. J., vol. 51, no. 2, pp. 429–454, 1972, doi: 10.1002/j.1538-7305.1972.tb01928.x.